28

Nanophotonics and Nanofibers

Limin Tong
State Key Laboratory of Modern Optical Instrumentation, and Department of Optical Engineering, Zhejiang University, Hangzhou 310027, China

Eric Mazur
Department of Physics and School of Engineering and Applied Sciences, Harvard University, Cambridge, Massachusetts, USA

28.1. INTRODUCTION

Nanophotonics is a fusion of photonics and nanotechnology, and is defined as nanoscale optical science and technology that includes nanoscale confinement of radiation, nanoscale confinement of matter, and nanoscale photoprocesses for nanofabrication [1–3]. While photonics has been widely used for fiber-optic data communication for decades, the application of nanotechnology for optical communication is an emerging technology. The basic motivation for incorporating photonics with nanotechnology is spurred by the requirement of increased integration of photonic devices for a variety of applications such as higher data transmission rates, faster response, lower energy consumption, and denser data storage [2]. For example, to reach an optical data transmission rate as high as 10 Tb/s, the size of photonic matrix switching devices should be reduced to 100-nm scale [4].

Historically, the nanotechnology was first proposed by Richard Feynman in his famous talk "There's Plenty of Room at the Bottom"—in the 1959 Annual Meeting of the American Physical Society [5] and has been thriving since the 1980s. Now, incorporated with physics, chemistry, materials, electronics, and biology, nanotechnology has spawned a number of new multidisciplinary areas. Compared with many other nano-incorporated fields such as nanoelectronics, nanophotonics is relatively new. In the past century, the application of nanotechnology in optics or photonics has usually been associated with the near-field scanning optical microscope (NSOM), with emphasis on near-field optics [6–8]. Recently, the rapid development of nanotechnology in photonics, together with

Handbook of Fiber Optic Data Communication: A Practical Guide to Optical Networking

ISBN: 978-0-12-374216-2

the emerging new frontiers such as surface plasmonics, optical antennas, negative-index metamaterials, and nanofibers in subwavelength optics [9], has greatly broadened the topic to cover a wider scope of light-matter interactions on the nanoscale, and brought new opportunities for future photonic applications, including optical communications, sensing, computing, and storage.

To illustrate this nano-induced potential for future fiber-optic data communication, this chapter provides brief introductions to nanophotonics and nanofibers, with the hope of providing insight to stimulate deeper understanding of this new frontier.

28.2. NANOPHOTONICS

The basic foundation of nanophotonics involves light–matter interaction on the nanometer scale, which is usually extended to subwavelength scale within the optical domain [3]. Physically speaking, in almost all nanophotonic processes concerned, light interacts with electrons (or, equivalently, electrons such as holes and excitons) inside the concerned materials. Therefore, theoretically most of the nanophotonic processes can be fully described by the Maxwell equations and the Schrödinger equation. However, the mesoscopic feature size of the nanophotonic structure, ranging from the atomic scale to the wavelength of the light, makes it difficult or impossible to precisely treat these systems the same way as individual constituents (e.g., a single or cluster of atoms) or large ensembles (e.g., a bulk material) without the perceptible or sometimes predominant optical near-field, surface, and quantum effects.

As has been mentioned, nanophotonics covers a broader area ranging from nanoscale optical engineering and quantum optics to biotechnology. Within the scope of this book, or more specifically on the technological side of optical communication, we are attempting to provide a conceptual introduction to some relative topics, including evanescent waves, surface plasmonics, and quantum confined effects. While we cannot claim comprehensive coverage of all relative topics, we hope that this work will serve as a valuable reference for the readers.

28.2.1. Optical Near-Field and Evanescent Waves

The near-field can be defined as the extension outside a given material of the field existing inside this material [10]. Generally, the amplitude of near-field maintains an evident value in the vicinity of the material boundary but decays very rapidly along the direction perpendicular to the interface, giving rise to the so-called evanescent wave character of the near-field. In optics, the field is manifested by the electromagnetic waves, and near-field optics deals with phenomena involving evanescent electromagnetic waves. In most cases, when the size of the structure goes to a subwavelength or a smaller scale, the effect

of evanescent field becomes significant, making it one of the primary topics of nanophotonics.

Historically, the research of optical evanescent waves can be traced back four hundred years [11], when Sir Isaac Newton investigated the frustrated total reflection of a prism. As schematically illustrated in Fig. 28.1, in one of his experiments, Newton placed a prism against a lens and observed that the light intensity transferred onto the lens was located on an area of the lens much larger than the point of contact. The result indicates that, when the air gap between the lens and the prism is very small, light confined by the prism tunnels through the gap and leaks into the lens, which is attributed to the existence of evanescent waves in the vicinity of the reflection surface.

Mathematically, evanescent fields in total reflection can be described using Maxwell's equations and boundary conditions of the electromagnetic fields. As a typical example, shown in Fig. 28.2 is reflection of light on a plane interface of two dielectric media with refractive indices of n_1 and n_2, respectively. Assume the incident light with the wavelength of λ to be a plane wave with an electric component $E_1 = E_{10}e^{i(k_{1x}x+k_{1z}z-\omega t)}$. When the incident angle θ_1 is larger than the critical angle θ_c [$\theta_c = \sin^{-1}(n_2/n_1)$], total reflection occurs with a penetration field ($z > 0$ region) $E_3 = E_{30}e^{i(k_{3x}x+k_{3z}z-\omega t)}$, where

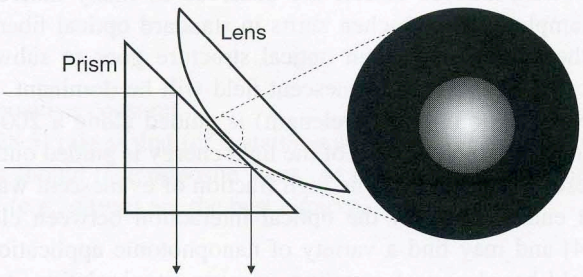

Figure 28.1 Schematic illustration of the frustrated total reflection of a prism.

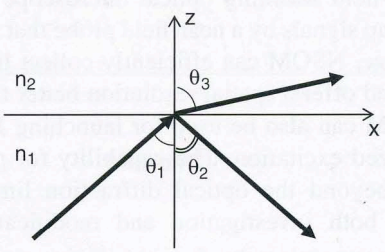

Figure 28.2 Reflection of light on a plane interface.

$$k_{3z} = k_3 \cdot \sqrt{1 - \sin^2(\theta_3)} = \frac{2\pi}{\lambda} \cdot \sqrt{1 - \frac{n_1^2 \sin^2(\theta_1)}{n_2^2}} \tag{28.1}$$

When $\theta_1 > \theta_c$, $\sqrt{1 - \frac{n_1^2 \sin^2(\theta_1)}{n_2^2}}$ is imaginary, Eq. (28.1) can be expressed as

$$k_{3z} = i\kappa = i\frac{2\pi}{\lambda} \cdot \sqrt{n_1^2 \sin^2(\theta_1) - n_2^2} \tag{28.2}$$

where κ is real. The penetration field is then written as

$$E_3 = E_{30} e^{-\kappa z} e^{i(k_{3x}x - \omega t)} \tag{28.3}$$

Therefore, E_3 is an evanescent field and decays exponentially along the z-direction with a penetration depth

$$d = \frac{1}{\kappa} = \frac{\lambda}{2\pi\sqrt{n_1^2 \sin^2(\theta_1) - n_2^2}} \tag{28.4}$$

For reference, with a green light (λ~500 nm) and an angle of incidence of 60°, assume n_1 and n_2 to be 1.5 (e.g., glass) and 1.0 (air); the penetration length d is about 100 nm.

Evanescent-field-induced effects are observed in many macroscopic structures. For example, Goos-Hänchen shifts in standard optical fibers [12]. However, when the feature size of an optical structure goes to subwavelength or nanometer scale, the effect of evanescent field will be dominant. For example, when a He-Ne laser (633-nm wavelength) is guided along a 200-nm-diameter air-clad silica nanofiber, over 90% of the light energy is guided outside the silica core as evanescent waves [13]. The high fraction of evanescent waves may lead to significant enhancement of the optical interaction between closely located structures [14] and may find a variety of nanophotonic applications, including evanescent-field-based optical coupling, sensing, manipulation, excitation, and nonlinear effects.

The characterization of evanescent fields has been greatly facilitated by the invention of the near-field scanning optical microscope (NSOM) [15]. When scanning and picking up signals by a near-field probe that is kept less than 10 nm away from the interface, NSOM can efficiently collect light energy carried by the evanescent field and offer a spatial resolution better than 50 nm. By operating it reversely, NSOM can also be used for launching light into a very small area for highly localized excitation. The capability for picking up evanescent waves and imaging beyond the optical diffraction limit makes the NSOM a powerful tool for both investigation and modification of nanophotonic structures.

28.2.2. Surface Plasmon Resonance

Surface plasmon resonance (SPR) is the collective oscillation of electrons on the interface between a metal and a dielectric medium. This kind of oscillation, highly localized on the surface of the metal-dielectric boundary, decays quickly along the direction perpendicular to the interface. One of the well-known early works on SPR was reported by R. H. Ritchie in 1957 [16], in which the plasma losses by fast electrons in thin metallic films were investigated theoretically. In 1970s, J. Shoenwald et al. experimentally observed the propagation of surface polaritons on a metal-air surface at optical frequencies [17]. Due to the low-loss feature of metals at infrared wavelength, they found that these localized surface waves could propagate over macroscopic distances. Recently, incorporated with nanotechnology, SPR has brought considerable changes in the optical properties of nanostructures, such as enhanced transmission in subwavelength aperture and optical waveguiding in metal nanoparticle chains [18–20].

A schematic illustration of SPR is shown in Fig. 28.3. Assume an interface located at $z = 0$ to be the interface of the two media with permittivities of ε_1 (Medium 1) and ε_2 (Medium 2), respectively. The surface wave propagated along y-direction. To keep the electromagnetic energy around the interface, the boundary conditions and the symmetry of the electric fields (i.e., the z-components of the electric field in the two half spaces should always take opposite signs) require that

$$\varepsilon_1 = -C\varepsilon_2 \tag{28.5}$$

where C is a positive constant.

Equation (28.5) means that for sustaining a surface wave, the permittivities of the two media should take opposite signs. At optical frequency, dielectric (e.g., air) and metal (e.g., silver) are the best choices.

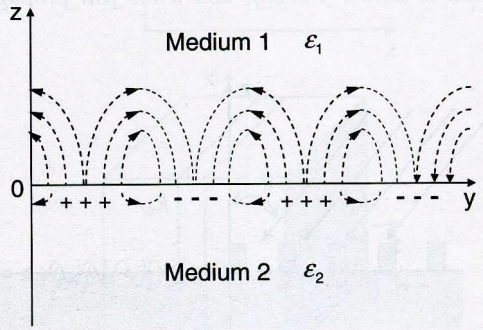

Figure 28.3 Schematic illustration of surface plasmon resonance (SPR).

By solving Maxwell's equations under appropriate boundary conditions, the dispersion relation for these surface waves can be obtained as [20]

$$k_{sp} = k_y = \frac{\omega}{c} \cdot \sqrt{\frac{\varepsilon_1 \varepsilon_2}{\varepsilon_1 + \varepsilon_2}} \tag{28.6}$$

Generally, the momentum of the surface wave (k_{sp}) obtained in Eq. (28.6) is larger than that of the light wave propagating in free space (i.e., in medium 1), indicating the difficulty for direct coupling between the free-space light and the surface waves.

To achieve efficient coupling between the light and the surface wave, there are several approaches for compensation of the momentum mismatch [17], among which the introduction of periodic structures is one of the most effective and practical approaches. As shown in Fig. 28.4, when a light beam is incident on a one-dimensional grating with a period of H, the momentum of light in the y-direction is

$$k_y - \frac{2\pi}{\lambda} \sin\theta \pm \frac{2\pi n}{H} \tag{28.7}$$

where θ is the angle of incidence, λ is the wavelength of the light, and n is an integer. The second term in the right side of Eq. (28.7) is the additional momentum from the grating, which can be used for compensating the momentum mismatch. To get a high coupling efficiency within the visible or near-infrared spectral range, the grating period H should be on a subwavelength or nanometer scale.

The potential of SPR for future optical data processing originates from its capability of utilizing low-dimensional surface waves to provide deep subwavelength or nanoscale confinement, guidance, and switch of light energy [21]. For example, in 2003, S. A. Maier et al. demonstrated light energy transport in metal nanoparticle plasmon waveguides at 570-nm wavelength [19]. The cross section of the particle chain is below 100 nm, and a 0.5-μm propagation length was

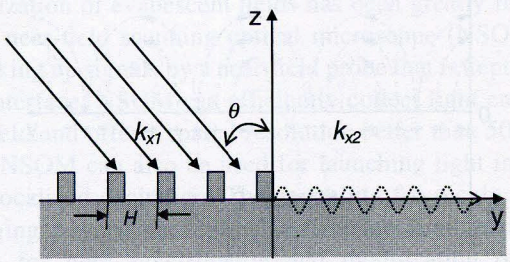

Figure 28.4 Schematic diagram of grating coupling between free-space light and surface plasmon waves.

observed. More recently, SPR-based photonic devices such as optical interferometers, filters, and resonators have been demonstrated [22, 23].

28.2.3. Quantum Confined Effects

Generally, the wave-like nature of the electrons becomes obvious when the dimension of the confinement approaches or becomes smaller than the de Broglie wavelength of the electron. In most cases, this kind of quantum confinement is obtained or enhanced by size reduction of the nanostructure, and can be used to control and sometimes introduce new optical properties of the nanostructures.

Nanostructurized inorganic semiconductor is one of the most important and widely used materials for manifestation of the quantum confinement effect, which provides an added dimension to the highly active area of "bandgap engineering" of the semiconductor bandgap [3]. So far, the quantum-confined structures of many different types of semiconductors have been demonstrated, such as quantum wells, quantum wires, quantum dots, and superlattices.

For a brief introduction, Fig. 28.5 shows a schematic illustration of a quantum well, in which a layer of a small bandgap semiconductor with thickness on the nanometer scale is sandwiched between two layers of a wider bandgap semiconductor. The layered structure provides the potential for confining the electrons and the holes, resulting in quantized energy levels of these charge carriers when their kinetic energies are lower than the potential provided by the well. In a simplest case that the potential well is a one-dimension box with infinite height, the energy of the electron in the conduction band is given as [3]

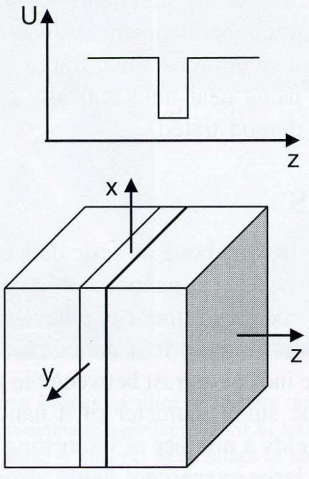

Figure 28.5 Schematic diagram of a quantum well.

$$E_{n,k_x,k_y} = E_C + \frac{n^2h^2}{8m_e^*l^2} + \frac{h^2(k_x^2 + k_y^2)}{8\pi^2 m_e^*} \tag{28.8}$$

where h is the Planck constant, l is width of the well, E_c is the lowest energy of the electron at the bottom of the conduction band, m_e^* is the effective mass of the electron, n is an integer larger than zero, and k_x and k_y are momentum of the electron in the x- and y-direction. The second term on the right-hand side represents the quantized energy. Since the minimum value of n is 1, the quantization increases the energy of the electron in the conduction band. For the hole in the valence band, the quantization decreases its energy because of its positive charge. Therefore, the bandgap of the semiconductor in the quantum well is increased and becomes size-dependent.

Besides the change of the energy, another important feature of quantum confined structure is the modification of the density of the states (DOS), which is also directly associated with the optical properties of the nanostructure. For example, in bulk materials, the DOS of an electron is zero at the bottom of the conduction band and is continuously increased with increasing energy, while in a quantum dot, the DOS is a series of discontinuous peaks. That means DOS has discrete values only at some allowed energy, which is similar to the energy level of an atom and makes the quantum dot an "artificial atom".

The quantum effects in nanostructures bring new opportunities for nanophotonic devices. For example, compared with heterostructure lasers without tight quantum confinement, quantum well lasers offer lower threshold, narrow spectral gain, and much higher modulation frequency [24]. Another example is the quantum cascade laser that relies on the intraband transition of electrons between subbands generated by quantum confinement in quantum well superlattices [25], which provides an excellent solution for the infrared laser source. More recently, nanophotonic NOT gates using near-field optically coupled quantum dots [26] have been experimentally demonstrated.

28.3. NANOFIBERS

Glass fiber is no doubt the backbone of optic data communication and optical networking [27]. Recent advances in nanophotonics have spurred efforts for the miniaturization of optical fibers and fiber-optic devices. When the diameter of a fiber goes well below 1 micrometer, it is called a nanofiber. The nanofiber is usually operated with large index contrast between the glass core and the cladding atmosphere (e.g., air). The small diameter of a nanofiber and the large core-cladding index contrast yields a number of interesting optical properties such as tight optical confinement, large evanescent fields, strong field enhancement, and large waveguide dispersions. An important motivation for nanoscale fiber optics

is its potential usefulness as building blocks in future micro- or nanophotonic devices for optical communications, sensors, and other purposes.

28.3.1. Nanofiber Fabrication

The optical nanofibers introduced here are fabricated by high-temperature taper drawing of standard optical fibers or bulk glasses, which is a top-down process that permits the fabrication of nanofibers with high uniformities [28–30]. Figure 28.6 shows typical electron microscope images of silica nanofibers drawn from standard optical fibers. For example, Fig. 28.6(a) is a scanning electron microscope (SEM) image of a 50-nm-diameter nanofiber; the high uniformity of its diameter is clearly seen. In Fig. 28.6(b), a 260-nm-diameter silica nanofiber is coiled up to show its length. Figure 28.6(c) is an SEM image of silica nanofibers with diameters ranging from 230 to 660 nm, all with high uniformities. To investigate the sidewall roughness, Fig. 28.6(d) shows a higher-magnification transmission electron microscope (TEM) image of a 330-nm-diameter silica nanofiber. No visible irregularity is found.

Besides the silica fiber, a variety of other types of glasses (e.g., phosphate, fluoride, and tellurite glasses) have also been drawn into

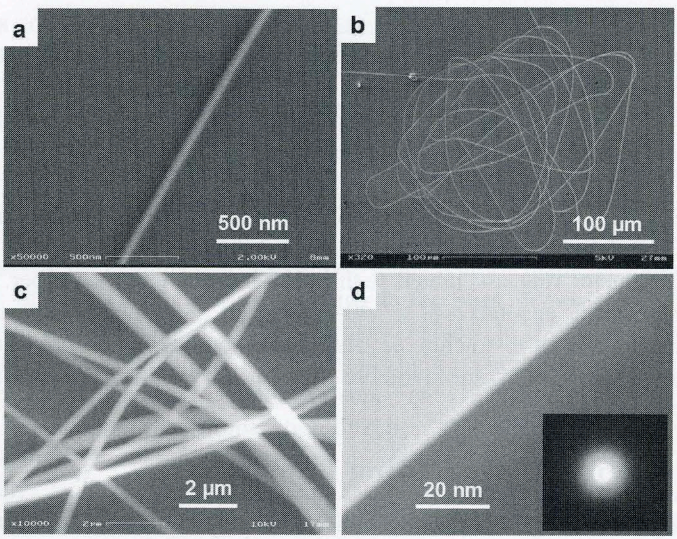

Figure 28.6 Electron microscope images of silica nanofibers taper-drawn from standard optical fibers. (a) SEM image of a 50-nm-diameter nanofiber. (b) SEM image of a coiled 260-nm-diameter nanofiber with a total length of about 4 mm. (c) SEM image of nanofibers with diameters ranging from 230 to 660 nm. (d) TEM image of the sidewall of a 330-nm-diameter nanofiber; the electron diffraction pattern (inset) shows that the fiber is amorphous. (Adapted from Ref. 28.)

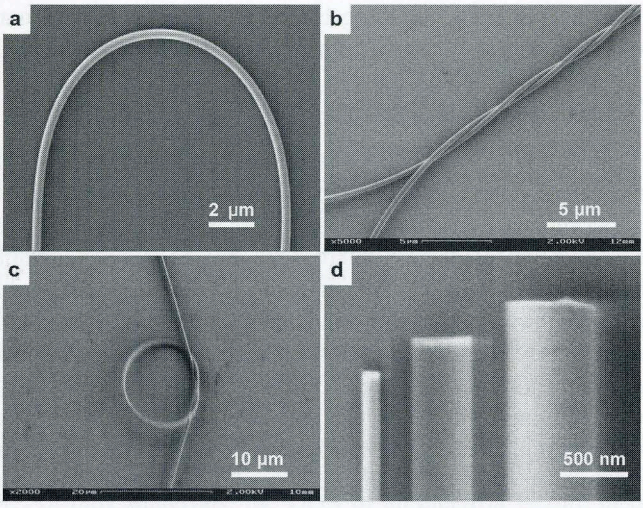

Figure 28.7 SEM images of silica nanofibers patterned with micromanipulation. (a) A bend of 5-μm radius formed with a 410-nm-diameter nanofiber. (b) Two twisted 400-nm-diameter nanofibers. (c) A 14.5-μm-diameter ring assembled using a 520-nm-diameter nanofiber. (d) Flat end faces of a 140-, 420- and 680-nm-diameter nanofibers obtained using a bend-to-fracture process.

highly uniform nanofibers, with diameters down to 50 nm and lengths up to millimeters [30].

Because of their high uniformities, taper-drawn nanofibers also show favorable mechanical properties for micromanipulation and processing. Shown in Fig. 28.7 are SEM images of silica nanofibers patterned with micromanipulation, in which Fig. 28.7(a) is a bend of 5-μm radius formed with a 410-nm diameter nanofiber, Fig. 28.7(b) is two twisted 400-nm-diameter nanofibers, Fig. 28.7(c) shows a 14.5-μm diameter ring assembled with a 520-nm-diameter nanofiber, and Fig. 28.7(d) shows flat end faces of a 140-, 420- and 680-nm diameter nanofibers obtained using a bend-to-fracture process [31]. The high flexibilities of the nanofibers shown in Fig. 28.7 are favorable for their practical applications in micro- and nanophotonic devices.

28.3.2. Optical Waveguiding Properties

Because of the cylindrical symmetry, the guiding behavior of an optical nanofiber can be obtained using analytical solutions of Maxwell's equations [13, 32]. Normalized propagation constants β/k_0 (also known as the effective index; here β is the propagation constant, and $k_0 = 2\pi/\lambda_0$) of the first four modes of air-clad silica nanofiber are shown in Fig. 28.8(a). When the normalized fiber diameter D/λ_0 falls below 0.73 (the dotted line indicates the cut-off condition for single mode), the

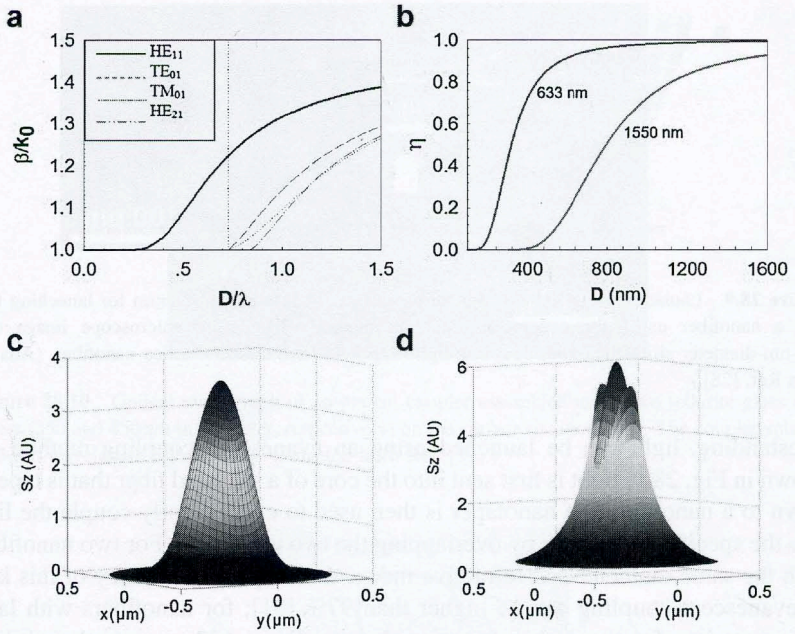

Figure 28.8 Optical wave-guiding properties of air-clad silica nanofibers. (a) Normalized propagation constants β/k_0 of the first four modes. The dotted line indicates the cutoff condition. (b) Fractional power of HE_{11} mode inside the core at 633- and 1550-nm wavelengths. (c) and (d) Z-component Poynting vector in 457- and 229-nm-diameter fibers at 633-nm wavelength, respectively. Mesh, inside silica core; gradient, outside the core.

fiber is a single-mode waveguide. Fig. 28.8(b) shows the fractional power of the fundamental mode (HE_{11}) inside the core at 633- and 1550-nm wavelengths, respectively. For example, at the single-mode cutoff diameter (D_{SM}), more than 80% of the light energy is guided inside the fiber, demonstrating its tight-confinement ability. When the fiber diameter reduces to 0.5 D_{SM}, for example, 229 nm at 633-nm wavelength, about 86% of light power propagates outside the fiber as evanescent waves. For comparison, Figs. 28.8(c) and 28.8(d) give the Poynting vector (along the propagation direction z) of the fundamental mode at 633-nm wavelength with fiber diameters of 457 nm (D_{SM}) and 229 nm (0.5 D_{SM}), respectively. Tight confinement is helpful to reduce the bending loss in a sharp bend; weak confinement, on the other hand, facilitates the light coupling from one wire to another. These favorable guiding properties make the nanofiber promising for building evanescent-coupling-based devices with ultra-compact sizes.

Experimentally, for a nanofiber that is connected to a standard fiber through the tapering region, light guided in the standard fiber can be directly squeezed into the nanofiber through the tapering region. For a nanofiber with both ends

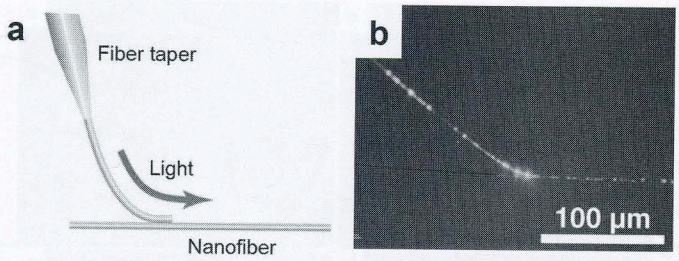

Figure 28.9 Launching light into an optical nanofiber. (a) Schematic diagram for launching light into a nanofiber using the evanescent coupling method. (b) Optical microscope image of a 390-nm-diameter silica nanofiber coupling light into a 450-nm-diameter silica nanofiber. (Adapted from Ref. [28].)

freestanding, light can be launched using an evanescent coupling method. As shown in Fig. 28.9, light is first sent into the core of a standard fiber that is tapered down to a nanofiber; the nanotaper is then used to evanescently couple the light into the specified nanofiber by overlapping the two in parallel. For two nanofibers with the same diameter and refractive index, the coupling efficiency of this kind of evanescent coupling can be higher than 97% [31]; for nanofibers with large difference in refractive index, for example, coupling a 633-nm-wavelength light from a silica nanofiber (1.46 in refractive index) to a tellurite nanofiber (2.0 in index), the coupling efficiency can go up to 90% when the fiber diameter and overlapping length are properly selected [14].

Because of their extraordinary uniformities, taper-drawn nanofibers guide light with low optical losses. Typical loss of taper-drawn glass nanofibers measured at the critical diameter for single-mode operation is lower than 0.1dB/mm [30], with the lowest loss of about 0.001dB/mm measured in silica nanofibers [33], which is much lower than the optical loss of other subwavelength-structures such as surface plasmon waveguides or nanowires fabricated with other methods. The low optical loss, tight optical confinement, strong evanescent field, high uniformity, and mechanical strength make nanofibers promising building blocks for micro- or nanophotonic components.

28.3.3. Device Applications

A variety of micro- or nanoscale photonic components or devices, including optical couplers, interferometers, resonators, and sensors, have been demonstrated using taper-drawn nanofibers [30, 31, 34–39]. Because of their small size, low optical loss, evanescent wave guiding, and mechanical flexibility, these devices show high potential for applications in optical communications and sensors.

Figure 28.10 shows a microscale optical coupler assembled from two tellurite glass nanofibers with diameters of 350 and 450 nm, respectively. When 633-nm-

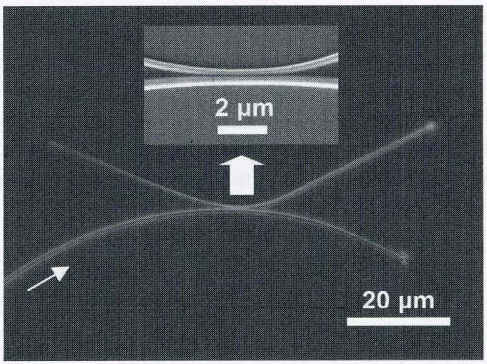

Figure 28.10 Optical micrograph of an optical coupler assembled using two tellurite glass nanofibers (350 and 450 nm in diameter, respectively) on the surface of silica glass. The coupler splits the 633-nm-wavelength light equally. (Adapted from Ref. [30].)

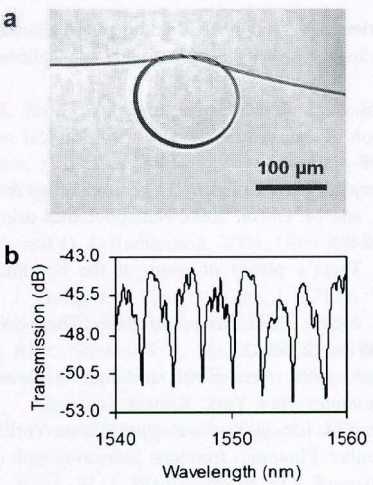

Figure 28.11 Nanofiber-assembled knot resonator. (a) Optical micrograph of a 150-μm-diameter microknot assembled with an 880-nm-diameter silica fiber. (b) Transmission spectrum of the microknot shown in (a).

wavelength light is launched into the bottom left arm, the coupler splits the flow of light in two, working as a 3-dB splitter with almost no excess loss. The overlap length of less than 5 μm is much shorter than the transfer length required by conventional fused couplers made from larger-diameter fiber tapers [40].

When tying a nanofiber into a loop or a knot, a microresonator can be obtained through the evanescent coupling at the joined area. For example, Fig. 28.11(a)

shows a 150-μm-diameter microknot assembled with an 880-nm-diameter fiber. The measured transmittance of this microknot for wavelengths near 1550 nm is shown in Fig. 28.11(b). The spectral response of the knot clearly shows optical resonances with a Q-factor higher than 1000. Recently, microcoil/loop resonators with Q-factors as high as 95,000 have been realized [41], and a proposed microcoil resonator with self-coupling turns is expected to display a Q-factor as high as 10^{10} [42].

Based on microresonators, a series of photonic devices can be realized. Recently, knot-resonator-based add-drop filters and lasers have been experimentally realized using micrometer-diameter silica fibers and rare-earth doped phosphate glass fibers [43, 44]. Rare-earth doped nanofiber ring lasers with much smaller sizes have been theoretically predicted [45], indicating the possibility to develop much more compact devices using nanofibers for optical communications and sensors.

REFERENCES

1. Shen, Y. Z., C. S. Friend, Y. Jiang, D. Jakubczyk, J. Swiatkiewicz, and P. N. Prasad. 2000. Nanophotonics: Interactions, materials, and applications. *J. Phys. Chem. B* 104: 7577–7587.
2. Ohtsu, M., K. Kobayashi, T. Kawazoe, S. Sangu, and T. Yatsui. 2002. Nanophotonics: Design, fabrication, and operation of nanometric devices using optical near fields. *IEEE J. Sel. Top. Quantum Electron.* 8:839–862.
3. Prasad, P. N. 2004. *Nanophotonics*. Hoboken, N.J.: John Wiley & Sons.
4. Kawazoe, T., T. Yatsui, and M. Ohtsu. 2006. Nanophotonics using optical near fields. *J. Non-Cryst. Solids* 352:2492–2495.
5. Feynman, R. P. 1992. There's plenty of room at the bottom. *J. Microelectromech. Syst.* 1:60–66.
6. Paesler, M. A., and P. J. Moyer. 1996. *Near-field optics: Theory, instrumentation, and applications*. New York: John Wiley & Sons.
7. Ohtsu, M., and H. Hori. 1999. *Near-Field nano-optics: From basic principles to nano-fabrication and nano-photonics*. New York: Kluwer Academic.
8. Kawata, S., M. Ohtsu, and M. Irie. 2002. *Nano-Optics*. New York: Springer.
9. Hecht, Jeff. 2005, September. Photonics frontiers: Subwavelength optics come into focus. *Laser Focus World.*
10. Girard, C., C. Joachim, and S. Gauthier. 2000. The physics of the near-field. *Rep. Prog. Phys.* 63:893–938.
11. de Fornel, F. 2001. *Evanescent waves: From Newtonian optics to atomic optics*. Berlin: Springer-Verlag.
12. Saleh, B. E. A., and M. C. Teich. 1991. *Fundamentals of photonics*. New York: John Wiley & Sons.
13. Tong, L. M., J. Y. Lou, and E. Mazur. 2004. Single-mode guiding properties of subwavelength-diameter silica and silicon wire waveguides. *Opt. Express* 12:1025.
14. Huang, K. J., S. Y. Yang, and L. M. Tong. 2007. Modeling of evanescent coupling between two parallel optical nanowires. *Appl. Opt.* 46:1429–1434.
15. Betzig, E., J. K. Trautman, T. D. Harris, J. S. Weiner, and R. S. Kostelak. 1991. Beating the diffraction barrier: Optical microscopy on a nanometer scale. *Science* 251:1468–1470.

16. Ritchie, R. H. 1957. Plasma losses by fast electrons in thin films. *Phys. Rev.* 106:874–881.
17. Shoenwald, J., E. Burstein, and M. Elson. 1973. Propagation of surface polaritons over macroscopic distances at optical frequencies. *Solid State Commun.* 12:185–189.
18. Ebbesen, T. W., H. J. Lezec, H. F. Ghaemi, T. Thio, and P. A. Wolff. 1998. Extraordinary optical transmission through sub-wavelength hole arrays. *Nature* 391:667–669.
19. Maier, S. A., et al. 2003. Local detection of electromagnetic energy transport below the diffraction limit in metal nanoparticle plasmon waveguides. *Nature Mater.* 2:229–232.
20. Barnes, W. L., A. Dereux, and T. W. Ebbesen. 2003. Surface plasmon subwavelength optics. *Nature* 424:824–830.
21. Maier, S. A. 2006. Plasmonics: Metal nanostructures for subwavelength photonic devices. *IEEE J. Sel. Top. Quantum Electron.* 12:1214–1220.
22. Bozhevolnyi, S. I., V. S. Volkov, E. Devaux, J. Y. Laluet, and T. W. Ebbesen. 2006. Channel plasmon subwavelength waveguide components including interferometers and ring resonators. *Nature* 440:508–511.
23. Volkov, V. S., S. I. Bozhevolnyi, E. Devaux, J. Y. Laluet, and T. W. Ebbesen. 2007. Wavelength selective nanophotonic components utilizing channel plasmon polaritons. *Nano Lett.* 7:880–884.
24. Zory, P. S. 1993. *Quantum well lasers*. New York: Academic Press.
25. Capasso, F., C. Gmachl, D. L. Sivco, and A. Y. Cho. 2002, May. Quantum cascade lasers. *Phys. Today* 34–40.
26. Kawazoe, T., K. Kobayashi, K. Akahane, M. Naruse, N. Yamamoto, and M. Ohtsu. 2006. Demonstration of nanophotonic NOT gate using near-field optically coupled quantum dots. *Appl. Phys. B* 84:243–246.
27. Mynbaev, D. K., and L. L. Scheiner. 2001. *Fiber-optic communications technology*, New York: Prentice Hall.
28. Tong, L. M., R. R. Gattass, J. B. Ashcom, S. L. He, J. Y. Lou, M. Y. Shen, I. Maxwell, and E. Mazur. 2003. Subwavelength-diameter silica wires for low-loss optical wave guiding. *Nature* 426:816–819.
29. Brambilla, G., V. Finazzi, and D. J. Richardson. 2004. Ultra-low-loss optical fiber nanotapers. *Opt. Express* 12:2258–2263.
30. Tong, L. M., L. L. Hu, J. J. Zhang, J. R. Qiu, Q. Yang, J. Y. Lou, Y. H. Shen, J. L. He, and Z. Z. Ye. 2006. Photonic nanowires directly drawn from bulk glasses. *Opt. Express* 14:82–87.
31. Tong, L. M., J. Y. Lou, R. R. Gattass, S. L. He, X. W. Chen, L. Liu, and E. Mazur. 2005. Assembly of silica nanowires on silica aerogels for microphotonic devices. *Nano Lett.* 5:259–262.
32. Snyder, A. W., and J. D. Love. 1983. *Optical waveguide theory*. New York: Chapman and Hall.
33. Leon-Saval, S. G., T. A. Birks, W. J. Wadsworth, P. St.J. Russell, and M. W. Mason. 2004. Supercontinuum generation in submicron fibre waveguides. *Opt. Express* 12:2864–2869.
34. Sumetsky, M., Y. Dulashko, and A. Hale. 2004. Fabrication and study of bent and coiled free silica nanowires: Self-coupling microloop optical interferometer. *Opt. Express* 12:3521–3531.
35. Sumetsky, M., Y. Dulashko, J. M. Fini, and A. Hale. 2005. Optical microfiber loop resonator. *Appl. Phys. Lett.* 86:161108.
36. Sumetsky, M. 2005. Uniform coil optical resonator and waveguide: transmission spectrum, eigenmodes, and dispersion relation. *Opt. Express* 13:4331–4340.
37. Lou, J., L. Tong, and Z. Ye. 2005. Modeling of silica nanowires for optical sensing. *Opt. Express* 13:2135–2140.
38. Polynkin, P., A. Polynkin, N. Peyghambarian, and M. Mansuripur. 2005. Evanescent field-based optical fiber sensing device for measuring the refractive index of liquids in microfluidic channels. *Opt. Lett.* 30:1273–1275.

39. Villatoro, J., and D. Monzón-Hernández. 2005. Fast detection of hydrogen with nano fiber tapers coated with ultra thin palladium layers. *Opt. Express* 13:5087–5092.
40. Kakarantzas, G., T. E. Dimmick, T. A. Birks, R. Le Roux, and P. St. J. Russell. 2001. Miniature all-fiber devices based on CO_2 laser microstructuring of tapered fibers. *Opt. Lett.* 26:1137–1139.
41. Sumetsky, M., Y. Dulashko, J. M. Fini, A. Hale, and D. J. DiGiovanni. 2005. Demonstration of the microfiber loop optical resonator. Optical Fiber Communication Conference, Postdeadline papers, Paper PDP10, Anaheim, Calif.
42. Sumetsky, M. 2004. Optical fiber microcoil resonator. *Opt. Express* 12:2303–2316.
43. Jiang, X. S., Y. Chen, G. Vienne, and L. M. Tong. 2007. All-fiber add–drop filters based on microfiber knot resonators. *Opt. Lett.* 32:1710–1712.
44. Jiang, X. S., Q. Yang, G. Vienne, Y. H. Li, L. M. Tong, J. J. Zhang, and L. L. Hu. 2006. Demonstration of microfiber knot laser. *Appl. Phys. Lett.* 89:143513.
45. Li, Y. H., G. Vienne, X. S. Jiang, X. Y. Pan, X. Liu, P. F. Gu, and L. M. Tong. 2006. Modeling rare-earth doped microfiber ring laser. *Opt. Express* 14:7073–7086.